Adsorption-controlled growth of Ga₂O₃ by suboxide molecular-beam epitaxy (F)

View Online   Export Citation   CrossMark

Patrick Vogt,[1,a)] (ID) Felix V. E. Hensling,[1] (ID) Kathy Azizie,[1] Celesta S. Chang,[2] (ID) David Turner,[3,4] Jisung Park,[1] (ID) Jonathan P. McCandless,[5] Hanjong Paik,[1,6] Brandon J. Bocklund,[7] (ID) Georg Hoffman,[8] Oliver Bierwagen,[8] (ID) Debdeep Jena,[1,5,9] Huili G. Xing,[1,5,9] (ID) Shin Mou,[3] David A. Muller,[2,9] Shun-Li Shang,[7] Zi-Kui Liu,[7] and Darrell G. Schlom[1,9,10,b)] (ID)

AFFILIATIONS

[1] Department of Materials Science and Engineering, Cornell University, Ithaca, New York 14853, USA
[2] School of Applied and Engineering Physics, Cornell University, Ithaca, New York 14853, USA
[3] Air Force Research Laboratory, Materials and Manufacturing Directorate, Wright Patterson AFB, Ohio 45433, USA
[4] Azimuth Corporation, 2970 Presidential Drive, Suite 200, Fairborn, Ohio 45324, USA
[5] School of Electrical and Computer Engineering, Cornell University, Ithaca, New York 14853, USA
[6] Platform for the Accelerated Realization, Analysis, and Discovery of Interface Materials (PARADIM), Cornell University, Ithaca, New York 14853, USA
[7] Department of Materials Science and Engineering, Pennsylvania State University, University Park, Pennsylvania 16802, USA
[8] Paul-Drude-Institut für Festkörperelektronik, Leibniz-Institut im Forschungsverbund Berlin e.V., Hausvogteiplatz 5–7, 10117 Berlin, Germany
[9] Kavli Institute at Cornell for Nanoscale Science, Ithaca, New York 14853, USA
[10] Leibniz-Institut für Kristallzüchtung, Max-Born-Str. 2, 12489 Berlin, Germany

a) Author to whom correspondence should be addressed: pv269@cornell.edu
b) Electronic mail: schlom@cornell.edu

ABSTRACT

This paper introduces a growth method—suboxide molecular-beam epitaxy (S-MBE)—which enables a drastic enhancement in the growth rates of Ga_2O_3 and related materials to over 1 µm h^{-1} in an adsorption-controlled regime, combined with excellent crystallinity. Using a Ga + Ga_2O_3 mixture with an oxygen mole fraction of $x(O) = 0.4$ as an MBE source, we overcome kinetic limits that had previously hampered the adsorption-controlled growth of Ga_2O_3 by MBE. We present growth rates up to 1.6 µm h^{-1} and 1.5 µm h^{-1} for Ga_2O_3/Al_2O_3 and Ga_2O_3/Ga_2O_3 structures, respectively, with very high crystalline quality at unparalleled low growth temperature for this level of perfection. We combine thermodynamic knowledge of how to create molecular beams of targeted suboxides with a kinetic model developed for the S-MBE of III–VI compounds to identify appropriate growth conditions. Using S-MBE, we demonstrate the growth of phase-pure, smooth, and high-purity homoepitaxial Ga_2O_3 films that are thicker than 4.5 µm. With the high growth rate of S-MBE, we anticipate a significant improvement to vertical Ga_2O_3-based devices. We describe and demonstrate how this growth method can be applied to a wide range of oxides. With respect to growth rates and crystalline quality, S-MBE rivals leading synthesis methods currently used for the production of Ga_2O_3-based devices.

I. INTRODUCTION

Molecular-beam epitaxy (MBE) involves the growth of epitaxial thin films from molecular beams. In "conventional" MBE, the molecular beams consist of elements. An example is the Ga (g) species that evaporate from a heated crucible containing Ga (ℓ) or the As₄ (g) species that evaporate from a heated crucible containing As (s), where g, ℓ, and s denote gaseous, liquid, and solid,

respectively. In gas-source MBE, the species in the molecular beams originate from gases that are plumbed into the MBE from individual gas cylinders, for example, arsine or phosphine. In metal–organic MBE, the species in the molecular beams are metal–organic molecules such as trimethylgallium or trimethylaluminum.[1] "Suboxide" MBE refers to an MBE growth process utilizing molecular beams of suboxides such as Ga_2O (g) or In_2O (g). We have applied this method to the growth of Ga_2O_3 thin films and find that it can produce epitaxial Ga_2O_3 films with greater crystalline perfection combined with much higher growth rates than currently demonstrated by any other MBE method for the growth of this material.

A. "Conventional" MBE of Ga_2O_3 and related materials

Gallium-sesquioxide (Ga_2O_3) synthesized in its different polymorphs [i.e., α-Ga_2O_3 (rhombohedral), β-Ga_2O_3 (monoclinic), γ-Ga_2O_3 (cubic spinel), ε-Ga_2O_3 (hexagonal), and κ-Ga_2O_3 (orthorhombic)] is an emerging semiconductor possessing promising features for unprecedented high-power electronics. This is due to its large band gap (~5 eV)[2,3] and very high breakdown field (up to 8 MV cm^{-1}).[4] The band gap of Ga_2O_3 may be widened by alloying Ga_2O_3 with Al_2O_3 to form $(Al_xGa_{1-x})_2O_3$.[3] The synthesis of $(Al_xGa_{1-x})_2O_3/Ga_2O_3$ heterostructures with high Al content x is desired for high-power transistors with large band gap offsets.[3,5,6]

It is known that the "conventional" MBE of Ga_2O_3—i.e., when supplying elemental Ga and active O species during growth—is strongly limited by the formation and subsequent desorption of its volatile suboxide Ga_2O.[7–11] In the adsorption-controlled regime (i.e., grown with an excess of Ga), the growth rate strongly decreases with increasing Ga flux, ϕ_{Ga}, because not enough oxygen is available to oxidize the physisorbed Ga_2O to Ga_2O_3 (s) and the Ga_2O desorbs from the hot substrate. At sufficiently high ϕ_{Ga}, film growth stops and even goes negative (i.e., the Ga_2O_3 film is etched).[8] This effect is enhanced as the growth temperature, T_G, increases due to the thermally activated desorption of Ga_2O from the growth surface. The enhanced, T_G-induced Ga_2O desorption leads to a decreasing growth rate even in the O-rich regime, resulting in a short growth rate plateau (the value of which is far below the available active O flux[12]), followed by an even further decreasing growth rate in the adsorption-controlled regime.[9,12,13] These effects, i.e., the O-deficiency induced and thermally activated desorption of suboxides,[9,11–13] are detrimental for the growth of III–VI (e.g., Ga_2O_3) and IV–VI (e.g., SnO_2) materials in the adsorption-controlled regime.

Nevertheless, the MBE of thin films in the adsorption-controlled growth regime is often desired for high crystal perfection,[14–16] smooth surface morphology,[17] avoiding undesired oxidation states,[18,19] or suppressing the formation of electrically compensating defects.[20,21]

The growth rate evolution of Ga_2O_3 is microscopically explained by a complex two-step reaction mechanism.[11,12] In the *first* reaction step, all Ga oxidizes to Ga_2O via the reaction

$$2Ga\,(a) + O\,(a) \longrightarrow Ga_2O\,(a,g), \qquad (1)$$
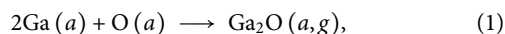
with adsorbate and gaseous phases denoted as a and g, respectively. The Ga_2O formed may either desorb from the growth surface (in the O-deficient regime or at elevated T_G) or be further oxidized to

Ga_2O_3 via a *second* reaction step through the reaction

$$Ga_2O\,(a) + 2O\,(a) \longrightarrow Ga_2O_3\,(s), \qquad (2)$$
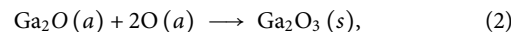
with the solid phase denoted as s.

This two-step reaction mechanism and the resulting Ga_2O desorption define the growth-rate-limiting step for the "conventional" MBE of Ga_2O_3 and related materials.[11,12] This results in a rather narrow growth window associated with low growth rates in the adsorption-controlled regime.[7–9,11] A similar growth-rate-limiting behavior, based on this two-step reaction mechanism, has also been reported for the growth of other III–VI (e.g., In_2O_3) and IV–VI (e.g., SnO_2) compounds by "conventional" MBE.[8,11,13] This two-step growth process for the growth of III–VI and IV–VI oxides by "conventional" MBE is fundamentally different from the single-step reaction mechanism of, for example, III–V[22–24] and II–VI[25] compounds. This difference in reaction kinetics can be attributed to the different electronic configurations of the compound constituents, resulting in different compound stoichiometries between III–VI and IV–VI compared with III–V and II–VI materials, respectively.

In the growth method introduced in this work, which we call *suboxide* MBE (*S*-MBE), we avoid the first reaction step (1) by directly supplying a Ga_2O (g) molecular beam to the growth front of the substrate surface. Using this approach, we bypass the growth-rate-limiting step of Ga_2O_3 by removing the O-consuming step to Ga_2O formation that occurs on the substrate in the "conventional" MBE growth of Ga_2O_3.[11,12] A related approach has been used by Ghose *et al.*[26,27] with Ga_2O provided from Ga_2O_3 source material heated to temperatures well in excess of 1600 °C to produce a molecular beam of Ga_2O for the growth of Ga_2O_3 films by MBE.[28] Motivated by known vapor pressure data of oxides[29] and their mixtures with the respective metals, e.g., Ga + Ga_2O_3,[30] as well as the possibility of decomposing Ga_2O_3 by Ga and SnO_2 by Sn under MBE conditions,[8] Hoffmann *et al.*[31] demonstrated how mixtures of Ga with Ga_2O_3 and Sn with SnO_2 provide MBE-relevant fluxes of Ga_2O and SnO, respectively, at source temperatures below 1000 °C. This prior work has grown films using suboxide molecular beams by MBE at growth rates <0.2 µm h^{-1}.[31,32]

As we demonstrate, *S*-MBE enables the synthesis of Ga_2O_3 in the highly adsorption-controlled regime, at growth rates >1 µm h^{-1} with unparalleled crystalline quality for Ga_2O_3/Al_2O_3 heterostructures as well as homoepitaxial Ga_2O_3 at relatively low T_G. The growth rate of *S*-MBE is competitive with other established growth methods used in semiconductor industry—such as chemical vapor deposition (CVD)[33] or metal–organic CVD (MOCVD)[34] —and, moreover, leads to better structural perfection of the obtained thin films. With this improved perfection, we expect an improvement of n-type donor mobilities in Ga_2O_3 thin films doped with Sn, Ge, or Si grown by *S*-MBE, as well. The relatively low T_G at which it becomes possible to grow high-quality films by *S*-MBE is a crucial enabler for material integration where temperatures are limited, e.g., back end of line (BEOL) processes.

Figure 1 illustrates a schematic of how the growth rates of III–V and III–VI compounds depend on cation fluxes during their MBE growth. In this figure, all growth rate axes are normalized by the respective anion flux. Figure 1(a) depicts the observed behavior for III–V compounds, e.g., GaN.[24] Figure 1(b) shows the observed behavior for III–VI compounds, e.g., Ga_2O_3, when the group III
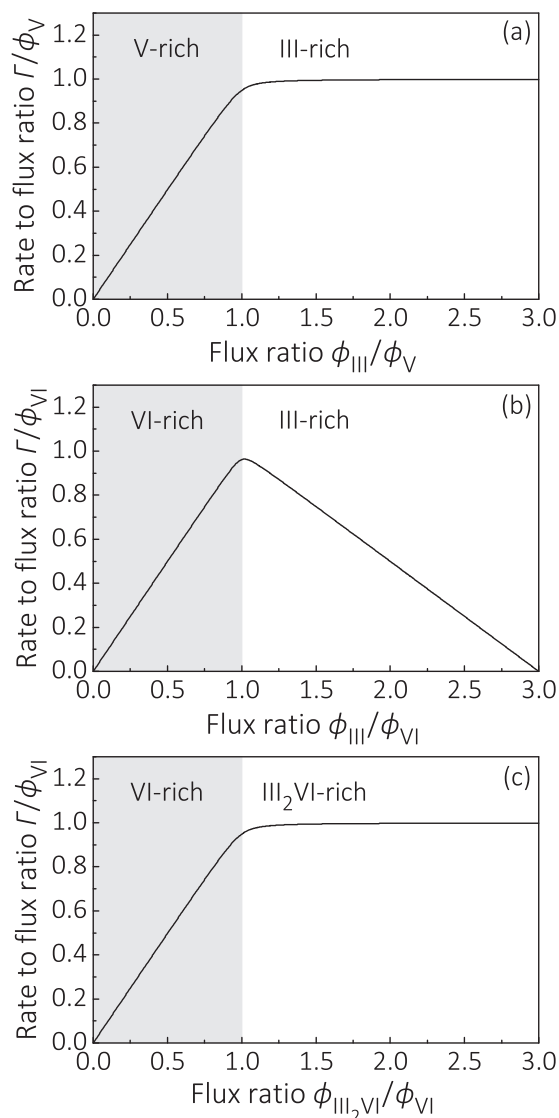
FIG. 1. (a) and (b) Schematic growth rate as observed for III–V (e.g., GaN)[24] and III–VI compounds (e.g., Ga_2O_3)[11] as a function of the III/V (e.g., ϕ_{Ga}/ϕ_N) and III/VI flux ratios (e.g., ϕ_{Ga}/ϕ_O), respectively. (c) Anticipated growth rate behavior of III–VI compounds (e.g., Ga_2O_3)[12] as a function of the III_2VI/VI flux ratio (e.g., ϕ_{Ga_2O}/ϕ_O). All schematic growth rate evolutions are normalized by the respective fluxes of active available group V (ϕ_V) and group VI elements (ϕ_{VI}). Each plot is at a constant T_G. Anion-rich and cation-rich regimes are indicated in gray and white, respectively.

cation is supplied by a molecular beam of the group III element (e.g., Ga).[8] In Fig. 1(c), the anticipated behavior for III–VI compounds is plotted, e.g., Ga_2O_3, when the group III element is supplied by a molecular beam of a III_2VI subcompound containing the group III constituent (e.g., Ga_2O).[12] The units of the horizontal and vertical axes are chosen to make the crossover between the anion-rich [gray areas in panels (a)–(c)] and cation-rich flux regimes [white areas in

panels (a)–(c)] to occur at values of unity. For the sake of simplicity, henceforth, we only discuss the reaction behavior of GaN and Ga_2O_3 in detail. We emphasize, however, that this discussion holds true for the MBE growth of AlN,[22] InN,[23] In_2O_3 (Refs. 8, 11, and 13), and other III–VI[11,35] and II–VI compounds.[25]

As drawn in Figs. 1(a)–1(c), the growth rate of GaN and Ga_2O_3 increases linearly with increasing ϕ_{Ga} in the N-rich [Fig. 1(a)] and O-rich regimes [Figs. 1(b) and 1(c)], respectively. Here, the incorporation of Ga is limited by the impinging ϕ_{Ga} or Ga_2O flux, ϕ_{Ga_2O} (i.e., Ga-transport and Ga_2O-transport limited growth regimes).

For GaN MBE [Fig. 1(a)], once the supplied ϕ_{Ga} exceeds the flux ϕ_N of active available N, the growth rate saturates, is independent of the ϕ_{Ga}/ϕ_N ratio, and is limited by ϕ_N and T_G. The measured plateau in the growth rate for GaN MBE in the Ga-rich regime results from its single-step reaction kinetics. Here, Ga reacts directly with activated N via the reaction[24]

$$Ga\,(a) + N\,(a) \longrightarrow GaN\,(s), \qquad (3)$$

and excess Ga either adsorbs onto or desorbs from the growth surface depending upon ϕ_N and T_G. Note that Eq. (3) and its discussion given in the text are identical for II–VI compounds (e.g., ZnO).

Figure 1(b) depicts the reaction kinetics of Ga_2O_3 in the Ga-rich regime (O-deficient growth regime) by supplying ϕ_{Ga}. Here, the growth rate linearly *decreases* with increasing ϕ_{Ga}, and the growth eventually stops at $\phi_{Ga} \geq 3\phi_O$ (in growth rate units). The fact that desorbing Ga_2O removes Ga *and* O from the growth surface—that cannot contribute to Ga_2O_3 formation—leads to the decreasing growth rate in the O-deficient growth regime.[8,9,11] This behavior is microscopically governed by the two-step reaction process, Eqs. (1) and (2),[11] and is fundamentally different from the single-step reaction kinetics, Eq. (3), governing the MBE of GaN [Fig. 1(a)].

In Fig. 1(c), the anticipated growth kinetics of Ga_2O_3 while using a Ga_2O beam is depicted, showing a constant growth rate in the Ga_2O-rich regime (i.e., in an excess of Ga_2O).[12] Excess Ga_2O (that cannot be oxidized to Ga_2O_3) either accumulates or desorbs off the growth surface *without* consuming or removing active O from its adsorbate reservoir—similar to the case presented for GaN in Fig. 1(a). Thus, with S-MBE, one may effectively achieve single-step reaction kinetics for Ga_2O_3 MBE [reaction (2)], as is the case for the growth of GaN by "conventional" MBE [reaction (3)].

The synthesis of III–V and II–VI materials with cation flux-independent growth rates in adsorption-controlled growth regimes—originating from their simple single-step reaction kinetics [e.g., reaction (3)]—is beneficial for device-relevant growth rate control and the improvement of their crystal properties.[36–38] Through the use of S-MBE, we convert the complex two-step reaction kinetics of III–VI [e.g., reactions (1) and (2)] and IV–VI compounds into simple single-step kinetics [e.g., (2)], the same as observed for III–V and II–VI materials. We therefore expect a similar growth behavior during S-MBE, i.e., constant growth rates in the adsorption-controlled regime, which are highly scalable by the provided active O flux. Such a regime should allow III–VI thin films (e.g., Ga_2O_3 and In_2O_3) and IV–VI films (e.g., SnO_2) to be grown much faster with excellent crystalline quality at relatively low T_G.
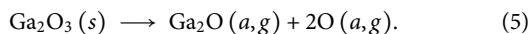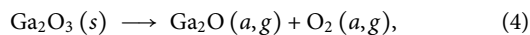
S-MBE utilizes molecular beams of suboxides and builds upon prior thermodynamic work and thin film growth studies. For example, molecular beams of the following suboxides have all been used in

MBE: Ga$_2$O,[26,27,32] GdO,[39,40] LuO,[40] LaO,[40] NdO,[41] PrO,[42,43] ScO,[44] SnO,[18,19,31,45,46] and YO.[39] Even before these MBE studies, thin films of the suboxides SiO,[47,48] SnO,[49–53] and GeO[54] had been deposited by thermal evaporation, exploiting the same underlying vapor pressure characteristics that make *S*-MBE possible. In some of these cases, the dominant species in the gas phase were not identified, but subsequent vapor pressure studies and thermodynamic calculations establish that they were suboxides.[29,55]

What is new about *S*-MBE is the recognition that the use of suboxide molecular beams reduces the complexity of the reaction kinetics of III–O and IV–O compounds from a complex two-step reaction mechanism[11,12] to a simple single-step reaction process. The growth kinetics during the *S*-MBE of III–O and IV–O compounds are equal to those of III–V and II–VI materials when they are grown by "conventional" MBE. Using this knowledge, *S*-MBE is applied in a targeted way to achieve epitaxial growth of desired oxides (e.g., Ga$_2$O$_3$) at very high growth rates in an adsorption-controlled regime. This leads to the benefits of the far simpler (from a growth kinetics, growth control, and growth standpoint) growth rate-plateau regime shown in Fig. 1(c) to be harnessed rather than the growth rate-decrease regime shown in Fig. 1(b) that has posed limits to the growth of Ga$_2$O$_3$ films and related materials by "conventional" MBE up to now.

II. DETAILED DESCRIPTION OF *S*-MBE

The use of a Ga$_2$O (g) molecular beam to grow Ga$_2$O$_3$ (s) thin films by MBE in the O-rich regime (i.e., in an excess of active O) has been demonstrated by placing a stoichiometric solid of the compound Ga$_2$O$_3$ into a crucible and using it as an MBE source.[26,27] Possible reactions that produce a Ga$_2$O molecular beam by the thermal decomposition of Ga$_2$O$_3$ are

$$\text{Ga}_2\text{O}_3\,(s) \longrightarrow \text{Ga}_2\text{O}\,(a,g) + \text{O}_2\,(a,g), \qquad (4)$$

$$\text{Ga}_2\text{O}_3\,(s) \longrightarrow \text{Ga}_2\text{O}\,(a,g) + 2\text{O}\,(a,g). \qquad (5)$$

One disadvantage of using Ga$_2$O$_3$ (s) as the MBE source is that Ga$_2$O$_3$ does not evaporate congruently. Our thermodynamic calculations indicate that when Ga$_2$O$_3$ (s) is heated to a temperature where the Ga$_2$O (g) has a vapor pressure of 0.1 Pa (a vapor pressure typical for MBE growth), the Ga$_2$O molecular beam contains only 98.0% Ga$_2$O molecules. The remaining 2% of the beam consists of Ga, O$_2$, and O species.

The other disadvantage of using Ga$_2$O$_3$ (s) as the MBE source is that quite high effusion cell temperatures are required to evolve appreciable $\phi_{\text{Ga}_2\text{O}}$; temperatures in excess of ~1600 °C,[28] ~1700 °C,[56] or ~1800 °C[26] have been used. At such high effusion cell temperatures, crucible choices become limited and prior researchers have used iridium crucibles.[26,27,32,56] Ga$_2$O$_3$ thin films synthesized utilizing an iridium crucible at an effusion cell temperature of ~1700 °C[56] were limited to growth rates <0.14 μm h^{-1} (Ref. 32) with ~5 × 10^{18} cm^{-3} iridium contamination in the grown Ga$_2$O$_3$ films.[56,57] These aspects of Ga$_2$O$_3$ compound sources hamper the synthesis of semiconducting Ga$_2$O$_3$ layers at growth rates exceeding 1 μm h^{-1} with device-relevant material properties. For comparison, the Ga + Ga$_2$O$_3$ mixture that we describe next and have used to grow Ga$_2$O$_3$ films at growth rates exceeding 1 μm h^{-1} provides a Ga$_2$O molecular beam that is 99.98% pure according to our thermodynamic

calculations. This is for the same Ga$_2$O vapor pressure of 0.1 Pa, which happens at a source temperature about 600 °C lower for this Ga + Ga$_2$O$_3$ mixture than for pure Ga$_2$O$_3$, enabling us to use crucibles that do not result in iridium-contaminated films.

Years ago as well as more recently, Ga + Ga$_2$O$_3$-mixed sources producing a Ga$_2$O molecular beam have been studied[30,31] and suggested as efficient suboxide sources for oxide MBE.[31,55] Using this mixed source, a Ga$_2$O (g) molecular beam is produced by the chemical reaction
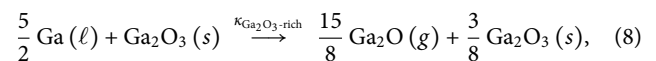
$$4\text{Ga}\,(\ell) + \text{Ga}_2\text{O}_3\,(s) \longrightarrow 3\text{Ga}_2\text{O}\,(s,g), \qquad (6)$$
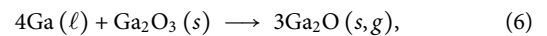
with the liquid phase denoted as ℓ. *S*-MBE uses the thermodynamic[30] and kinetic[8] properties of Ga + Ga$_2$O$_3$ mixtures favoring reaction (6) under MBE conditions.

For the *S*-MBE of Ga$_2$O$_3$, we explored Ga-rich and Ga$_2$O$_3$-rich mixtures of Ga + Ga$_2$O$_3$ with stoichiometries

$$5\text{Ga}\,(\ell) + \text{Ga}_2\text{O}_3\,(s) \xrightarrow{\kappa_{\text{Ga-rich}}} 3\,\text{Ga}_2\text{O}\,(g) + \text{Ga}\,(\ell) \qquad (7)$$

and

$$\frac{5}{2}\,\text{Ga}\,(\ell) + \text{Ga}_2\text{O}_3\,(s) \xrightarrow{\kappa_{\text{Ga}_2\text{O}_3\text{-rich}}} \frac{15}{8}\,\text{Ga}_2\text{O}\,(g) + \frac{3}{8}\,\text{Ga}_2\text{O}_3\,(s), \qquad (8)$$

respectively. The latter mixture has an oxygen mole fraction of $x(\text{O}) = 0.4$, and the properties of this Ga$_2$O$_3$-rich mixture are described below. The corresponding reaction rate constants $\kappa_{\text{Ga-rich}}$ and $\kappa_{\text{Ga}_2\text{O}_3\text{-rich}}$ define the production rate of Ga$_2$O (g) at a given temperature T_{mix} of the Ga + Ga$_2$O$_3$ mixture.

The flux of Ga$_2$O (g) in the molecular beam emanating from the mixed Ga + Ga$_2$O$_3$ sources is significantly larger than that of Ga (g)[30,58] emanating from the same source. This is also true under MBE conditions.[31,55] The resulting high ratio of Ga$_2$O/Ga ≫ 1 provides a more controllable and cleaner growth environment than accessible by decomposing a stoichiometric Ga$_2$O$_3$ source, which produces molecular beam ratios of Ga$_2$O/Ga, Ga$_2$O/O$_2$, and Ga$_2$O/O. Hence, the growth surface of the substrate during film growth using *S*-MBE is exposed to controllable and independently supplied molecular beams of Ga$_2$O and reactive O adsorbates.

We have experienced that a Ga$_2$O$_3$-rich mixture enables higher T_{mix} and higher, stable Ga$_2$O (g) molecular beams than a Ga-rich mixture. Thus, Ga$_2$O$_3$-rich mixtures enable higher growth rates by *S*-MBE than Ga-rich mixtures. This experimental observation is confirmed by our thermodynamic calculations of the phase diagram of Ga (ℓ) + Ga$_2$O$_3$ (s) mixtures, which we describe next.

The calculated Ga–O phase diagram in Fig. 2 shows that at T_{mix} below the three-phase equilibrium of gas + Ga (ℓ) + Ga$_2$O$_3$ (s) around 907 K, a two-phase region of Ga (ℓ)+Ga$_2$O$_3$ (s) forms, which does not change with respect to temperature or oxygen mole fraction between 0 and 0.6. Note that all thermodynamic calculations in the present work were performed using the Scientific Group Thermodata Europe (SGTE) substance database (SSUB5)[60] within the Thermo-Calc software.[61] For $T_{\text{mix}} > 907$ K, the two-phase regions are gas + Ga (ℓ) when the mole fraction of oxygen is below 1/3, corresponding to what we refer to as Ga-rich mixtures, and gas + Ga$_2$O$_3$ (s) when the mole fraction of oxygen is between 1/3 and 0.6, which we refer to as Ga$_2$O$_3$-rich mixtures. These two-phase
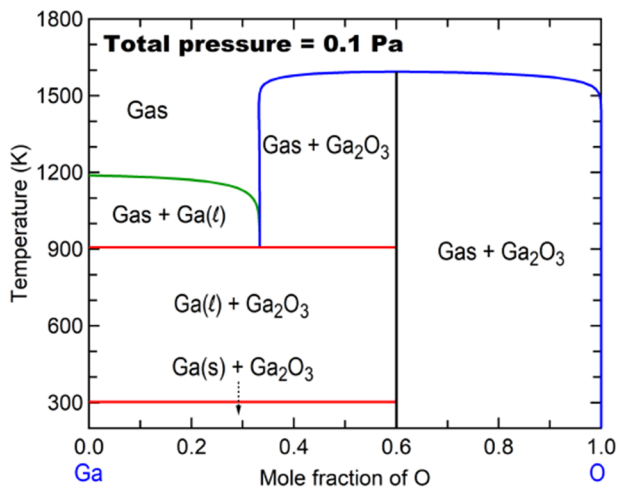
FIG. 2. Ga–O temperature-composition phase diagram under constant pressure P = 0.1 Pa. Calculations of this phase diagram at higher pressures are shown in Ref. 59.
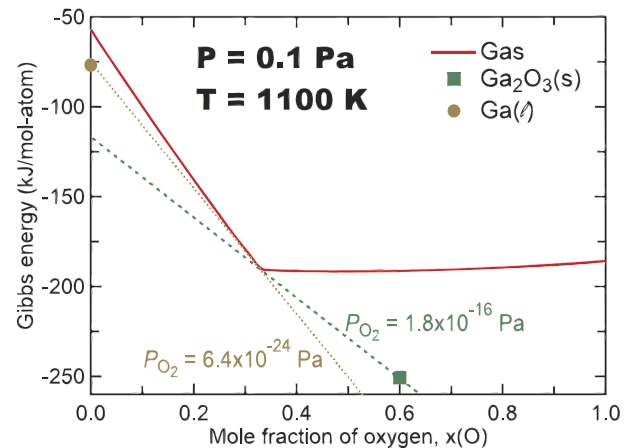

FIG. 4. Gibbs energies of the gas, Ga(ℓ), Ga$_2$O$_3$(s) phases at temperature T = 1100 K and total pressure P = 0.1 Pa. The brown dotted line shows the activity (or partial pressure) of oxygen when $0 < x(O) < 0.33$. In this range, the gas phase is in equilibrium with Ga(ℓ), and the activity of oxygen is 6.4×10^{-24} Pa. The green dashed line corresponds to the case where $0.33 < x(O) < 0.6$. In this range, the gas phase is in equilibrium with Ga$_2$O$_3$(s), and the activity of oxygen is $P_{O_2} = 1.8 \times 10^{-16}$ Pa. This difference in the partial pressure of O$_2$ between the two regimes is huge and shows the advantage of growing Ga$_2$O$_3$ films from Ga$_2$O$_3$-rich (Ga + Ga$_2$O$_3$) mixtures.

regions become a single gas-phase region at a T_{mix} of (907–1189) K for Ga-rich mixtures and at (907–1594) K for Ga$_2$O$_3$-rich mixtures, respectively. All of these phase transition temperatures decrease with decreasing pressure,[59] as shown in the pressure vs temperature ($P - T$) phase diagrams in Fig. 3.

To contrast the difference between Ga-rich vs Ga$_2$O$_3$-rich mixtures, we have performed additional thermodynamic calculations at oxygen mole fractions of $x(O)$ = 0.2 and $x(O)$ = 0.4. These two chosen oxygen mole fractions correspond to Ga-rich and Ga$_2$O$_3$-rich mixtures, respectively. In Figs. 3(a) and 3(b), the solid (red) lines denote the three-phase equilibrium between gas+Ga (ℓ)+Ga$_2$O$_3$ (s); these are identical at $x(O)$ = 0.2 and $x(O)$ = 0.4. The dotted (black) lines denote the equilibrium between the gas and gas + Ga (ℓ)

phase regions for $x(O)$ = 0.2 as well as the gas and gas + Ga$_2$O$_3$ (s) phase regions for $x(O)$ = 0.4, i.e., their respective boiling temperature/pressure.

Figure 4 shows Gibbs energies of the gas, Ga(ℓ), Ga$_2$O$_3$(s) phases at temperature T = 1100 K and total pressure P = 0.1 Pa. There are seven distinct atomic and molecular species in the gas phase: Ga, Ga$_2$, GaO, Ga$_2$O, O, O$_2$, and O$_3$. The kink in the Gibbs energy of the gas phase at $x(O)$ = 0.33 corresponds to the composition of the Ga$_2$O species because it is the major species in the gas
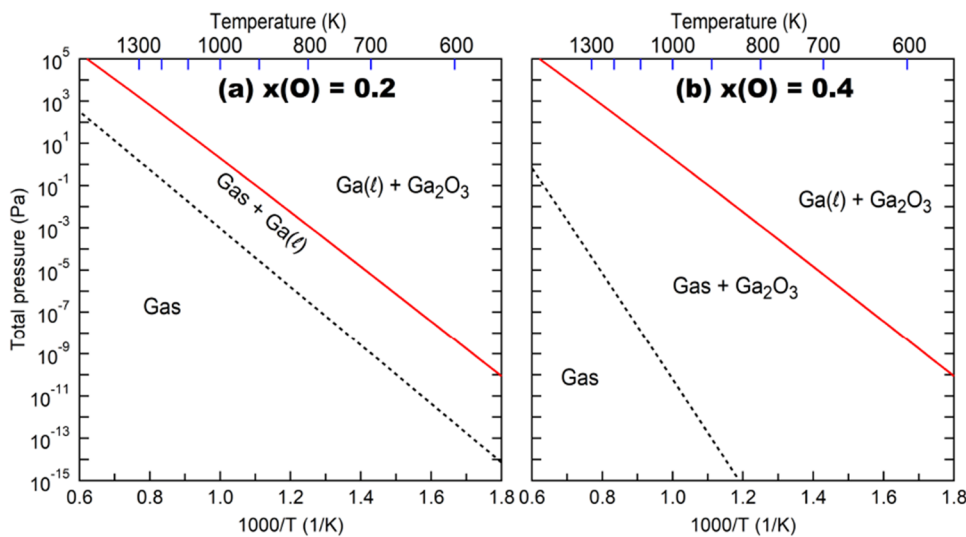
FIG. 3. Ga–O pressure vs temperature ($P - T$) phase diagrams at fixed mole fractions of oxygen of $x(O)$ = 0.2 [panel (a)] and $x(O)$ = 0.4 [panel (b)]. These oxygen mole fractions are chosen to illustrate the difference between (a) Ga-rich mixtures and (b) Ga$_2$O$_3$-rich mixtures.
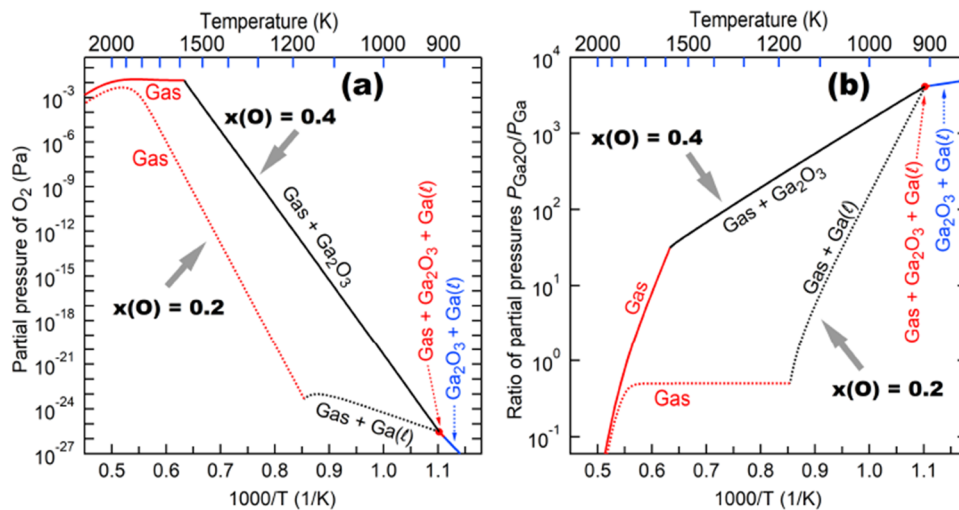
FIG. 5. (a) Partial pressure of oxygen and (b) ratio of the partial pressure of Ga_2O to that of Ga plotted as a function of temperature with the total pressure being 0.1 Pa for the mole fractions of oxygen at $x(O) = 0.2$ (dotted lines) and $x(O) = 0.4$ (solid lines), respectively. These oxygen mole fractions are chosen to illustrate the difference between Ga-rich mixtures [$x(O) = 0.2$] and Ga_2O_3-rich mixtures [$x(O) = 0.4$].

phase. It can be seen that the values of the oxygen activity in the gas + Ga (ℓ) vs in the gas + Ga_2O_3 (s) regions differ by more than seven orders of magnitude, i.e., 6.4×10^{-24} Pa vs 1.8×10^{-16} Pa as indicated by the brown and green common tangent lines in Fig. 4.

In Fig. 5(a), the partial pressure of oxygen in the gas phase is plotted as a function of temperature (for a total pressure of 0.1 Pa) for a Ga-rich mixture at $x(O) = 0.2$ and a Ga_2O_3-rich mixture at $x(O) = 0.4$. It can be seen that the oxygen partial pressure in the Ga_2O_3-rich mixture at $x(O) = 0.4$ is orders of magnitude higher than that at $x(O) = 0.2$ at relevant MBE growth temperatures. For example, the value of the partial pressures of oxygen at $T_{mix} = 1000$ K at $x(O) = 0.2$ is 5.6×10^{-25} Pa and at $x(O) = 0.4$ is 4.5×10^{-21} Pa. The higher oxygen activity of Ga_2O_3-rich mixtures compared with Ga-rich mixtures makes it easier to form fully oxidized Ga_2O_3 thin films. At lower total pressure, all lines shift to lower temperatures.

Furthermore, our thermodynamic calculations plotted in Fig. 5(b) show the ratio of the partial pressures of Ga_2O to Ga in the gas phase as a function of the temperature of a Ga-rich mixture [$x(O) = 0.2$] and of a Ga_2O_3-rich mixture [$x(O) = 0.4$], where the total pressure is fixed at 0.1 Pa. The ratio of the partial pressures of Ga_2O to Ga in a Ga-rich mixture with $x(O) = 0.2$ is much lower than this ratio in a Ga_2O_3-rich mixture with $x(O) = 0.4$. For example, the P_{Ga_2O}/P_{Ga} ratio is 158 in a Ga-rich mixture [$x(O) = 0.2$] and 1496 in a Ga_2O_3-rich mixture [$x(O) = 0.4$] at $T_{mix} = 1000$ K. The higher Ga_2O/Ga ratios at higher T_{mix} are another reason why Ga_2O_3-rich mixtures are preferred. Higher Ga_2O/Ga ratios and the higher purity of the Ga_2O molecular beam [99.98% Ga_2O according to our calculations at $x(O) = 0.4$] mean that the Ga_2O_3 films are formed by a single-step reaction [reaction (2)] and that reaction (1) is bypassed.

We used Ga metal (7N purity) and Ga_2O_3 powder (5N purity) for the Ga + Ga_2O_3 mixtures, loaded them into a 40 cm^3 Al_2O_3 crucible, and inserted it into a commercial dual-filament, medium temperature MBE effusion cell. After mounting the effusion cell to our Veeco GEN10 MBE system and evacuating the source, we heated it up, outgassed the mixture, and set our desired Ga_2O flux for the growth of Ga_2O_3. We measured the flux of the Ga_2O (g) molecular beam reaching the growth surface prior to and after growth using

a quartz crystal microbalance. The 10×10 mm^2 substrates were back-side coated with a 10 nm thick Ti adhesion layer followed by 200 nm of Pt, enabling the otherwise transparent substrates to be radiatively heated during MBE growth. For S-MBE growth the substrate was held within a substrate holder made of Haynes® 214® alloy, and loaded into the growth chamber. The growth temperature T_G was measured by an optical pyrometer operating at a wavelength of 1550 nm. To determine the surface crystal phases during growth, *in situ* high-energy electron diffraction (RHEED) using 13 keV electrons was utilized. After growth x-ray reflectivity (XRR), optical reflectivity in a microscope (ORM),[62] scanning electron microscopy (SEM), scanning transmission electron microscopy (STEM), and secondary-ion mass spectrometry (SIMS) were used to accurately measure the thicknesses of homoepitaxial (ORM, SEM, SIMS, and SEM) and heteroepitaxial (XRR, ORM, SEM, STEM, and SIMS) grown Ga_2O_3 films to determine the growth rate. X-ray diffraction was performed using a four-circle x-ray diffractometer with Cu $K\alpha_1$ radiation.

III. RESULTS FOR Ga_2O_3 USING S-MBE

A. Growth rates and growth model

Figure 6 plots the growth rate of Ga_2O_3 as a function of ϕ_{Ga_2O} at different T_G and constant ϕ_O. The growth rates obtained follow the anticipated growth kinetics depicted in Fig. 1(c). In the adsorption-controlled regime, an increase in ϕ_{Ga_2O} (at otherwise constant growth parameters) does *not* lead to a decrease in the growth rate as observed for "conventional" Ga_2O_3 MBE [Fig. 1(b)][7,9] but instead results in a constant growth rate: a growth rate-plateau. The data clearly show that we have overcome the growth-rate-limiting step by using a Ga_2O (g) suboxide molecular beam while reducing the complexity of the Ga_2O_3 reaction kinetics from a two-step [Eqs. (1) and (2)] to a single-step [Eq. (2)] reaction mechanism.

The reaction kinetics of S-MBE for the growth of Ga_2O_3 (s) can be described in a similar way as "conventional" III–V [e.g., reaction (3)] and II–VI MBE. We therefore set up a simple reaction-rate
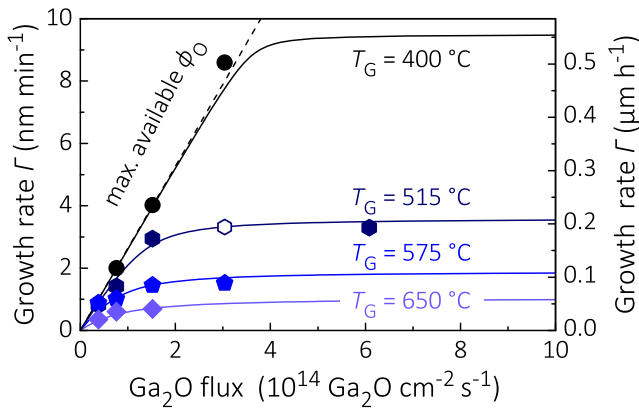
FIG. 6. Measured growth rate of $Ga_2O_3(\bar{2}01)/Al_2O_3(0001)$ as a function of ϕ_{Ga_2O} at different T_G (as indicated in the figure). Solid lines are fits of our model, Eqs. (9)–(11), to the data. A flux of ϕ_O was provided by an oxidant—a mixture of O_2 and approximately 80% O_3[63]—supplied continuously during growth at a background pressure of 1×10^{-6} Torr. The dashed line reveals the transition between O-rich and Ga_2O-rich growth regimes and indicates the maximum available O flux (which equals the growth rate value of the plateau) for Ga_2O to Ga_2O_3 conversion at a given T_G.

model describing the growth of Ga_2O_3 (s) by S-MBE (this same model applies to other III–VI and IV–VI compounds, as well),

$$\frac{dn_{Ga_2O}}{dt} = \phi_{Ga_2O} - \kappa_{Ga_2O}\, n_{Ga_2O}\, n_O^2 - \gamma_{Ga_2O}\, n_{Ga_2O}, \quad (9)$$

$$\frac{dn_O}{dt} = \sigma\phi_O - 2\,\kappa_{Ga_2O}\, n_{Ga_2O}\, n_O^2 - \gamma_O\, n_O, \quad (10)$$

$$\frac{dn_{Ga_2O_3}}{dt} = \Gamma = \kappa_{Ga_2O}\, n_{Ga_2O}\, n_O^2. \quad (11)$$

The Ga_2O_3, Ga_2O, and O adsorbate densities are denoted as $n_{Ga_2O_3}$, n_{Ga_2O}, and n_O, respectively. Their time derivative is described by the operator d/dt. The reaction rate constant κ_{Ga_2O} kinetically describes the growth rate Γ of Ga_2O_3 (s) on the growth surface. The desorption rate constants of Ga_2O and O adsorbates are denoted as γ_{Ga_2O} and γ_O, respectively.

The flux of available O adsorbates, for Ga_2O to Ga_2O_3 oxidation at a given T_G, is determined by its sticking coefficient σ on the Ga_2O_3 growth surface and is described by a sigmoid function

$$\sigma(T_G) = \left(1 + \sigma_0 \exp\left(-\frac{\Delta\sigma}{k_B T_G}\right)\right)^{-1}, \quad (12)$$

with dimensionless pre-factor σ_0 and energy $\Delta\sigma$. Equation (12) reflects the decreasing probability of O species to adsorb as T_G is increased. This leads to an effectively lower surface density of active O for Ga_2O oxidation and thus to lower growth rates.

We find that σ does not depend on the concentration of active O and only weakly on the partial pressure of active O (values not shown in this work). Thus, the active O may be scaled up or down by either changing the concentration of O_3 in the O_3 beam or by

changing the partial pressure of O_3 in the chamber. Note that O_3 supplies O to the surface of the growing film when it decomposes by the reaction: O_3 (g) → O_2 (g) + O (g). A similar behavior of an increasing desorption or recombination rate of active O species with increasing T_G has also been observed during O plasma-assisted MBE using elemental Ga and O molecular beams.[9,12,13]

Based on this model, we scaled up ϕ_O in order to achieve Ga_2O_3 (s) growth rates that exceed 1 μm h^{-1}. Figure 7(a) demonstrates our fastest (to date) growth rate of 1.6 μm h^{-1} of a β-Ga_2O_3 thin film grown on Al_2O_3(0001), at $T_G = 500$ °C. For comparison, the data point plotted as a hollow hexagon (see also Fig. 6) shows the highest possible growth rate at a five times lower active ϕ_O and similar T_G. This result demonstrates, scaling up the active O enables S-MBE to scale up the growth rates of Ga_2O_3 thin film exceeding 1 μm h^{-1}
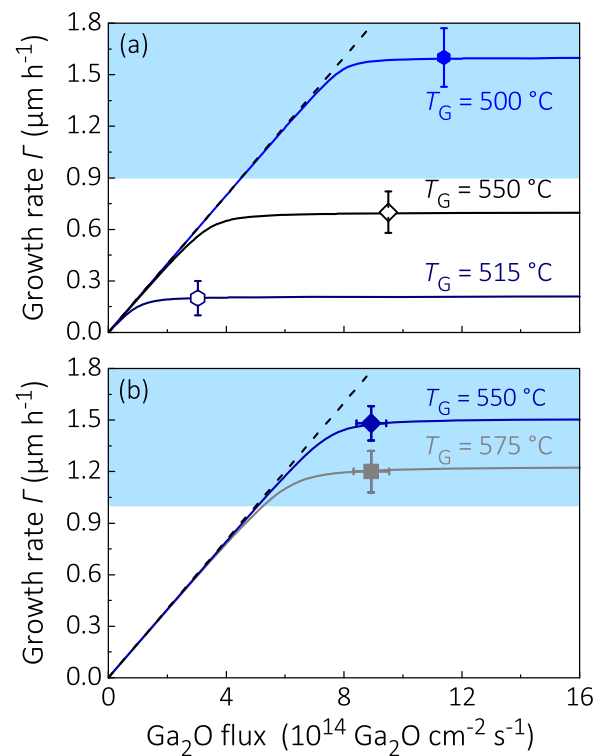
**FIG. 7**. (a) Examples of measured growth rates of 1.6 μm h^{-1} (solid hexagon), 0.7 μm h^{-1} (hollow diamond), and 0.2 μm h^{-1} (hollow hexagon; the same data point is shown in Fig. 6) of $Ga_2O_3(\bar{2}01)$ grown on Al_2O_3(0001) at ϕ_{Ga_2O} of 11.4, 9.5, and 3.0 × 10^{14} Ga_2O molecules cm^{-2} s^{-1}, respectively. The oxygen flux was provided by an oxidant (O_2 + 80% O_3) background pressure of 5 × 10^{-6} Torr (solid hexagon and hollow diamond) as well as 1 × 10^{-6} Torr (hollow hexagon). (b) Examples of measured growth rates of 1.5 μm h^{-1} (solid diamond) and 1.2 μm h^{-1} (solid square) of Ga_2O_3(010) grown on Ga_2O_3(010) at ϕ_{Ga_2O} = 8.4 × 10^{14} Ga_2O molecules cm^{-2} s^{-1}. The oxygen flux was provided by an oxidant (O_2 + 80% O_3) background pressure of 5 × 10^{-6} Torr. Growth temperatures, T_G, are indicated in the figure. Lines are estimations from our model, Eqs. (9)–(11). The dashed line shows the estimated intersection between the O-rich to the Ga_2O-rich growth regime. The blue shaded area indicates the adsorption-controlled growth rate-regime only accessible by S-MBE with growth rates ≥1 μm h^{-1}.

in the adsorption-controlled regime. In addition, the growth rate values plotted in Fig. 7(b) were obtained by homoepitaxial growth of β-Ga$_2$O$_3$(010) on β-Ga$_2$O$_3$(010). The growth rate of Ga$_2$O$_3$ on Ga$_2$O$_3$(010) is 2.1 times larger than the growth rate on Al$_2$O$_3$(0001) at similar growth conditions—e.g., as plotted in Fig. 7(a) (hollow diamond) and Fig. 7(b) (solid diamond), respectively. This result suggests that the growth rate of S-MBE grown on Ga$_2$O$_3$(010) and other surfaces of Ga$_2$O$_3$ may vastly exceed 1 μm h^{-1} in the adsorption-controlled regime. The higher growth rate of Ga$_2$O$_3$(010) compared with Ga$_2$O$_3$($\bar{2}$01) is similar to what has been observed during the "conventional" MBE of Ga$_2$O$_3$.[45,64] Fluctuations in T_G and ϕ_{Ga_2O} for different samples and, e.g., during the long duration growth of the "thick" sample (>3 h), are considered by the standard deviations of the measured values of T_G and ϕ_{Ga_2O}, as given in Fig. 7.

B. Structural properties

We investigated the impact of variable growth conditions (i.e., ϕ_{Ga_2O}, ϕ_O, and T_G) on the structural perfection of epitaxial Ga$_2$O$_3$ (s) films grown on Al$_2$O$_3$(0001) and Ga$_2$O$_3$(010) substrates. Figure 8 shows θ–2θ x-ray diffraction (XRD) scans of selected Ga$_2$O$_3$ films—the same samples depicted in Fig. 7(a) (solid blue hexagon and hollow hexagon). The reflections of the films coincide with the
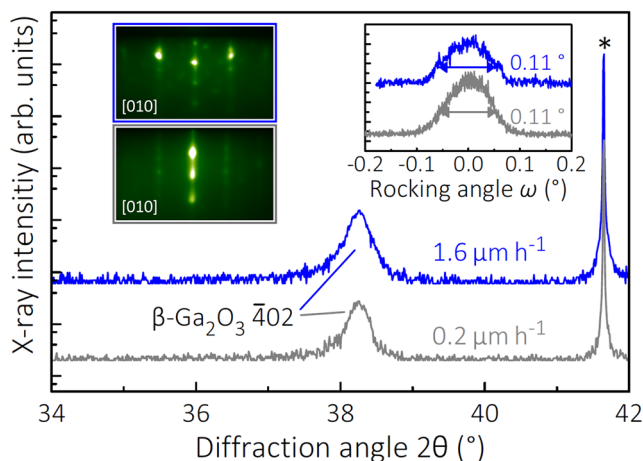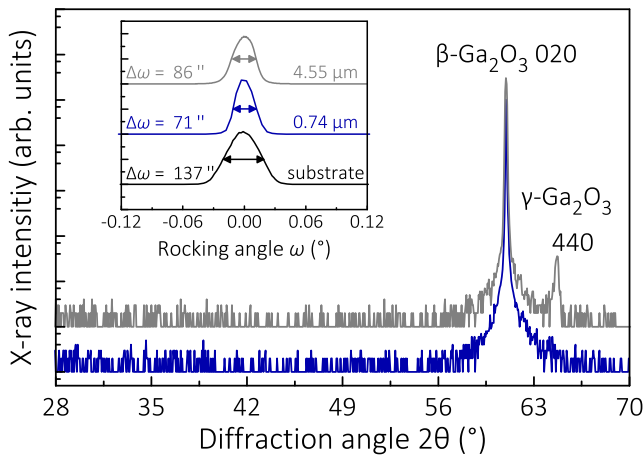

FIG. 8. Longitudinal XRD scans recorded for Ga$_2$O$_3$ films grown on Al$_2$O$_3$(0001) single-crystal substrates in the adsorption-controlled regime. The blue line corresponds to a film with a thickness of d = 0.15 μm grown at ϕ_{Ga_2O} = 11.4 × 10^{14} Ga$_2$O molecules cm^{-2} s^{-1}, where ϕ_O was provided by an oxidant (O$_2$ + 80%O$_3$) background pressure of 5 × 10^{-6} Torr [see also solid blue hexagon in Fig. 7(a)]. The gray line corresponds to a Ga$_2$O$_3$ film with thickness d = 0.05 μm grown at ϕ_{Ga_2O} = 3.0 × 10^{14} Ga$_2$O molecules cm^{-2} s^{-1}, where ϕ_O was provided by an oxidant (O$_2$ + 80%O$_3$) background pressure of 1 × 10^{-6} Torr [see also gray hollow hexagon in Fig. 7(a)]. T_G was 500 °C and 515 °C for the samples depicted as blue and gray lines, respectively. The reflections from the Ga$_2$O$_3$ film are identified to originate from the monoclinic β-phase,[65] as indicated in the figure. (Inset) Transverse XRD scans across the $\bar{4}$02 peak with their FWHM indicated in the figure (same value for both films). The 0006 peaks of the Al$_2$O$_3$ substrates are marked by an asterisk. RHEED images taken at the end of the growth along the [010] azimuth of the Ga$_2$O$_3$ films grown at growth rates of 1.6 μm h^{-1} and 0.2 μm h^{-1} are outlined by the blue and gray boxes, respectively.

β-Ga$_2$O$_3$ phase grown with their ($\bar{2}$01) plane parallel to the (0001) plane of the Al$_2$O$_3$ substrate. The inset shows transverse scans (rocking curves) across the symmetric $\bar{4}$02 reflection of the same layers. The full width at half maxima (FWHM) in ω of the profiles is a measure of the out-of-plane mosaic spread of the Ga$_2$O$_3$ layer. The obtained $\Delta\omega$ = 0.11° ≈ 400″ (arc sec) does not change with the growth rate and is particularly remarkable since β-Ga$_2$O$_3$($\bar{2}$01) films grown on Al$_2$O$_3$(0001), using elemental Ga[7,66] or compound Ga$_2$O$_3$ sources,[27] usually show much broader line profiles in their out-of-plane crystal distributions (from $\Delta\omega$ ≈ 0.23°[27] to $\Delta\omega$ ~ 1.00°).[7] Thus, the profiles in Fig. 8 reveal a well-oriented and high quality epitaxial Ga$_2$O$_3$($\bar{2}$01) thin film. Furthermore, reflection high-energy electron diffraction (RHEED) and XRR measurements reveal a sharp and well-defined interface between Ga$_2$O$_3$($\bar{2}$01) and Al$_2$O$_3$ as well as a relatively smooth surface morphology obtained by S-MBE. We note that in the highly adsorption-controlled regime at lower T_G, the accumulation of Ga$_2$O adsorbates (crystallites) on the growth surface may occur, similar to the formation of Ga droplets during GaN growth.[36] This effect is indicated by the slightly spotty RHEED image (outlined by the blue square) in Fig. 8. We have not yet optimized the growth for Ga$_2$O$_3$($\bar{2}$01) films on Al$_2$O$_3$(0001) with thicknesses ≫1 μm and have not mapped all growth regimes (e.g., Ga$_2$O "droplet" formation at very high ϕ_{Ga_2O}). Further investigations of the structural perfection and electrical properties of Ga$_2$O$_3$ grown by S-MBE need to be performed. This could be particularly interesting for the growth of Ga$_2$O$_3$ (s) at even higher Ga$_2$O (g) fluxes, which push even further into the adsorption-controlled regime.

We used S-MBE to grow homoepitaxial β-Ga$_2$O$_3$(010) films on β-Ga$_2$O$_3$(010) substrates. Figure 9 shows the θ–2θ XRD scans of two selected Ga$_2$O$_3$(010) films grown under the same growth conditions. The θ–2θ XRD profiles of the Ga$_2$O$_3$(010) film with thickness d = 0.74 μm (plotted in blue) and the one of the substrate (data not shown) coincide. The Ga$_2$O$_3$(010) layer with d = 4.55 μm (depicted in gray) also shows small contributions of the meta stable γ-Ga$_2$O$_3$ phase. The inset of Fig. 9 shows the respective rocking curves across the symmetric 020 reflections of the same films, as plotted in the main graph of Fig. 9. The obtained FWHM of the rocking curve of the film with d = 0.74 μm and d = 4.55 μm is comparable and narrower than the one obtained for the bare Ga$_2$O$_3$(010) substrate (depicted as a black line). [Note that the measured XRD spectra were obtained on different 10 × 10 mm^2 substrates, which were all cut from the same 1 in. diameter Ga$_2$O$_3$(010) wafer from Synoptics.] We attribute the different rocking curve widths measured to the non-uniformity in the crystalline perfection across the 1 in. diameter Ga$_2$O$_3$(010) substrate on which these measurements were made.

STEM of the "thick" film with d = 4.55 μm [the same sample as plotted as a gray line in Fig. 9 and solid square in Fig. 7(b)] are shown in Figs. 10(a)–10(e). The epilayer shows a clear, uniform, and single-crystalline β-Ga$_2$O$_3$(010) film. Defects such as dislocations or strain fields are not observed throughout this sample, indicating the very high crystal quality of this film. Only a thin γ-Ga$_2$O$_3$(110) layer at the top of the surface of the Ga$_2$O$_3$(010)/Ga$_2$O$_3$(010) homoepitaxial film can be seen, as marked by white circles in Figs. 10(b), 10(d), and 10(e). The 440 γ-Ga$_2$O$_3$ peak measured by XRD is attributed to this thin surface phase, which may increase with increasing film thickness and T_G. The formation of a γ-Ga$_2$O$_3$ surface phase has also been

FIG. 9. Longitudinal XRD scans recorded for Ga_2O_3 films grown on $Ga_2O_3(010)$ single-crystal substrates in the adsorption-controlled regime. The gray and blue lines correspond to Ga_2O_3 films with thicknesses of $d = 4.55\ \mu m$ and $d = 0.74\ \mu m$, respectively. The reflections of the films coincide with the β-$Ga_2O_3(010)$ phase grown with their (010) plane parallel to the plane of the substrate. (Inset) Transverse scans across the 020 peak of the same samples with their FWHM indicated in the figure. For comparison, a transverse scan of a single-crystalline $Ga_2O_3(010)$ substrate is also shown. The $Ga_2O_3(010)$ films (gray and blue) were grown at $\phi_{Ga_2O} = 8.9 \times 10^{14}$ Ga_2O molecules cm^{-2} s^{-1} and $T_G = 550\,°C$ and $T_G = 575\,°C$, respectively, where ϕ_O was provided by an oxidant ($O_2 + 80\%$ O_3) background pressure of 5×10^{-6} Torr. The surface morphologies of the "thin" ($d = 0.74\ \mu m$) and "thick" ($d = 4.55\ \mu m$) $Ga_2O_3(010)$ films are depicted in Figs. 11(a) and 11(c). The growth rates of the "thin" and "thick" films are indicated by the solid diamond and solid square, respectively, in Fig. 7(b).

observed during the growth of β-Ga_2O_3 by "conventional" MBE and might be an intrinsic issue for the homoepitaxy of $Ga_2O_3(010)$.[67]

    The surface morphology of $Ga_2O_3(010)$ films grown by S-MBE at growth rates $>1\ \mu m\ h^{-1}$ was investigated by atomic force microscopy (AFM) and is plotted in Figs. 11(a)–11(c). The root mean square (rms) roughness of the "thin" film with $d = 0.74\ \mu m$ is lower than the one measured for the "thick" film with $d = 4.1\ \mu m$ grown at similar conditions. The thick film with $d = 4.55\ \mu m$ grown at $T_G = 575\,°C$ shows a smoother surface, indicating that the thickness of the film does not influence the surface morphology detrimentally. This evolution in the rms roughness follows the same trend as observed by XRD scans of the same layers (blue and gray lines in the inset of Fig. 9), i.e., no decrease in crystalline quality with increasing film thickness of the $Ga_2O_3(010)/Ga_2O_3(010)$ structures was observed. We note that the difference in surface morphology seen in Figs. 11(a) and 11(b) may be caused by the slightly different off-cuts and crystal qualities among the bare β-$Ga_2O_3(010)$ substrates used, similar to the observed spread in rocking curves widths, as shown in Fig. 9.

C. Impurities

    We investigated the incorporation of impurities into the $Ga_2O_3(010)$ thin films grown with growth rates $> 1\ \mu m\ h^{-1}$ by SIMS. Figure 12 shows the SIMS profile of the same film as plotted in Fig. 7 (solid square) and Figs. 10 and 11(c). This profile reveals that the Ga_2O_3-rich (Ga + Ga_2O_3) mixtures employed lead to
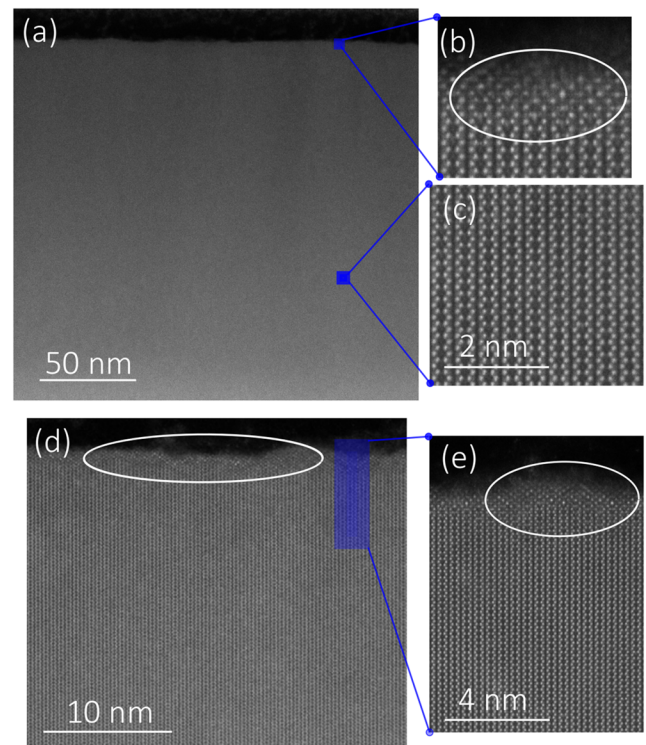
FIG. 10. (a)–(e) STEM images along the [001] zone axis of the $Ga_2O_3(010)$ "thick" film grown at $1.2\ \mu m\ h^{-1}$ with thickness $4.55\ \mu m$ [this is the same sample depicted by the solid square in Fig. 7(b) and gray line in Fig. 9]. The surface morphology of this film is shown in Fig. 11(c). No large-scale defects or dislocations are observed within this layer. The Ga_2O_3 films consist only of the β-$Ga_2O_3(010)$ phase, except for a γ-Ga_2O_3 phase at the top surface [highlighted by a white circle in (b), (d), and (e)].

$Ga_2O_3(010)$ thin films with very low impurity incorporation. Only a slight increase of B ~ 10^{16} cm^{-3} is detected. This impurity likely originates from our use of an Al_2O_3 crucible for the Ga_2O_3-rich (Ga + Ga_2O_3) mixture. We note that we have also used pyrolytic boron nitride (pBN) crucibles for the Ga + Ga_2O_3 mixture but find high concentrations of B in the grown films by SIMS (~10^{20} B cm^{-3}) when the background pressure of a mixture of $O_2 + 80\%O_3$ is $P_O = 5 \times 10^{-6}$ Torr. We attribute this to the oxidation of the surface of the pBN crucible to B_2O_3 at the high oxidant pressures used. At the $T_{mix} = 1020\,°C$ used for growth, the vapor pressure of B_2O_3 is significant.[55] The small Si and Al peaks measured at the film–substrate interface originate from unintentional incorporated Si and Al at the substrate surface. Note that we have tried Ga_2O-polishing (for the first time) to remove the Si from the surface prior to growth. Our observation is that Ga_2O-polishing does not provide the same reduction in Si contamination at the sample surface as can be accomplished by Ga-polishing.[68] All other detected impurities in the epilayer, i.e., Si (SIMS detection limit signal, $S_{Si} = 5 \times 10^{15}$ cm^{-3}), Fe ($S_{Fe} = 1 \times 10^{15}$ cm^{-3}), Sn ($S_{Sn} = 5 \times 10^{14}$ cm^{-3}), Al ($S_{Al} = 2 \times 10^{16}$ cm^{-3}), In ($S_{In} = 2 \times 10^{14}$ cm^{-3}) (not shown), and C ($S_C = 5 \times 10^{16}$ cm^{-3}) (not shown) in the film are below the detection limit of the cation standards used.
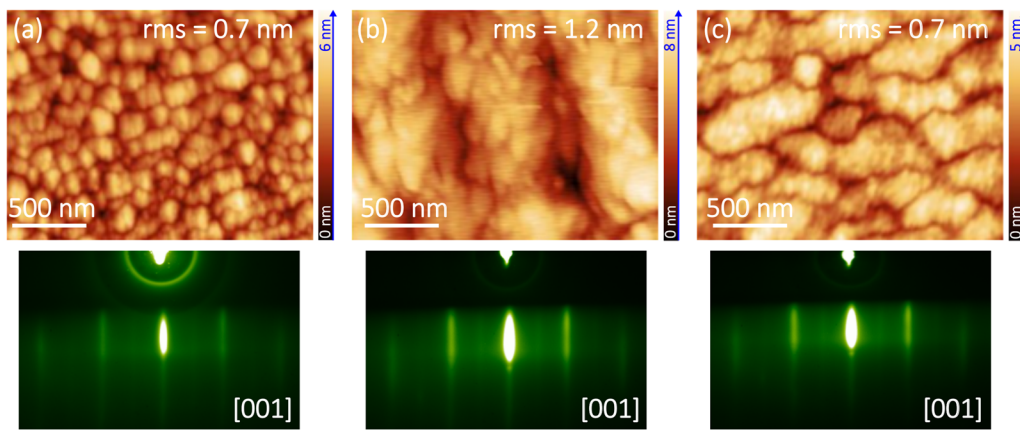
FIG. 11. (a)–(c) Surface morphologies obtained by AFM for $Ga_2O_3(010)$ surfaces grown by S-MBE. The rms roughness of the surfaces is indicated on the figures. The XRD patterns of the same layers as shown in (a) and (c) are plotted in Fig. 9 as blue and gray lines, respectively. In Fig. 7, the growth rates of the films shown in (a) and (b) (blue diamond) as well as (c) (gray square) are depicted. The thicknesses of the films in (a)–(c) are $d = 0.74$ μm, $d = 4.1$ μm, and $d = 4.55$ μm, respectively. Films shown in (a) and (b) were grown under similar growth conditions. T_G was set to 550 °C for the films shown in (a) and (b) and to $T_G = 575$ °C for the film plotted in (c). RHEED images of the corresponding Ga_2O_3 film taken at the end of growth along the [001] azimuth are displayed below the respective AFM images.

Our SIMS results show that the low effusion cell temperatures and Ga_2O_3-rich $(Ga + Ga_2O_3)$ mixtures employed for S-MBE—in order to produce the high Ga_2O fluxes used to grow Ga_2O_3 with growth rates exceeding >1 μm h^{-1}—do not lead to significant impurity incorporation into the grown $Ga_2O_3(010)$ films. This is an advantage of S-MBE compared with the growth Ga_2O_3 from a crucible containing pure Ga_2O_3. Using a Ga_2O_3 compound source at extremely high effusion cell temperatures (~1700 °C)[56] not only produces a flux containing a relatively low Ga_2O molecular beam resulting in low Ga_2O_3 film growth rates but also results in films contaminated with iridium.[32,56,57] Nonetheless, electrical transport

properties are extremely sensitive to impurities, and measurements of mobility in doped Ga_2O_3 films grown by S-MBE remain to be performed. It could turn out that a higher purity Ga_2O_3 powder will be needed than the 5N Ga_2O_3 powder we have used in this study.

D. Summary

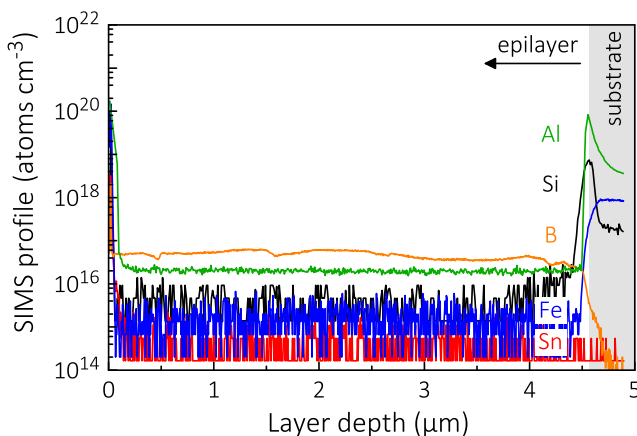The growth rates we have achieved by S-MBE are more than one order of magnitude faster than what has been reported for the growth of Ga_2O_3 films from pure Ga_2O_3 sources.[32]

The quality of the homoepitaxial β-$Ga_2O_3(010)$ films (with thicknesses > 4.5 μm) assessed by XRD (Fig. 9), STEM (Fig. 10), AFM (Fig. 11), and SIMS (Fig. 12) reveal that S-MBE with growth rates > 1 μm h^{-1} is competitive to other industrial relevant synthesis methods [such as (MO)CVD] for the growth of vertical Ga_2O_3-based structures with thicknesses in the μm-range.

Based on our model and experimental results, we anticipate growth rates up to 5 μm h^{-1} on $Ga_2O_3(010)$ and other growth surfaces to be possible by S-MBE. This estimation is based on the physical MBE limit: the mean free path λ of the species (e.g., Ga_2O and O_3) emanating from their sources to the target. In our estimate, we have used an upper limit for the O partial pressure of $P_O \sim 2 \times 10^{-4}$ Torr (resulting in $\lambda \sim 0.1$ m)[69] and a lower T_G limit of $T_G \geq 725$ °C [required for the adsorbed species (e.g., Ga_2O and O) to crystallize into a homoepitaxial film of Ga_2O_3 grown at a high growth rate].

FIG. 12. SIMS of a $Ga_2O_3(010)$ thin film grown at 1.2 μm h^{-1} [this is the same sample depicted by the solid square in Fig. 7(b)]. The atomic structure of this film and its surface morphology are shown in Figs. 10(a)–10(e) and 11(c), respectively. No significant impurity incorporation could be detected. Gray and white areas show the SIMS profile of the $Ga_2O_3(010)$ thin film and the Fe-doped $Ga_2O_3(010)$ substrate, respectively.

IV. OUTLOOK AND ALTERNATIVES OF S-MBE

We have demonstrated the growth of high quality Ga_2O_3 (s) thin films by S-MBE in the adsorption-controlled regime using $Ga(\ell) + Ga_2O_3(s)$ mixtures. The high growth rate ≫ 1 μm h^{-1} and unparalleled crystalline quality of the homoepitaxial and heteroepitaxial structures obtained (with $d \gg 1$ μm) suggest the possibility of unprecedented mobilities of Ga_2O_3 thin films containing n-type donors (Sn, Ge, Si) grown by S-MBE.

We have also developed Sn + SnO$_2$ and Ge + GeO$_2$ mixtures in order to produce SnO (g) and GeO (g) beams for use as n-type donors in Ga$_2$O$_3$-based heterostructures. Furthermore, we have grown SnO$_2$ using a Sn + SnO$_2$ mixture.[31] Moreover, we have grown Ga$_2$O$_3$ doped with SnO using Ga$_2$O and SnO beams and achieved controllable Sn-doping levels in these Ga$_2$O$_3$ films. Nevertheless, the improvement of the n-type mobilities obtained during S-MBE, at growth rates >1 µm h^{-1}, still needs to be demonstrated and shown to exceed the state-of-the-art mobilities in Ga$_2$O$_3$ films grown by "conventional" MBE.[70]

Our comprehensive thermodynamic analysis of the volatility of 128 binary oxides plus additional two-phase mixtures of metals with their binary oxides,[55] e.g., Ga + Ga$_2$O$_3$, have led us to recognize additional systems appropriate for growth by S-MBE. This thermodynamic knowledge coupled with our understanding of the S-MBE growth of Ga$_2$O$_3$ enabled us to develop In + In$_2$O$_3$ and Ta + Ta$_2$O$_5$ mixtures from which we have grown high-quality bixbyite In$_2$O$_3$ and In$_2$O$_3$:SnO$_2$ (ITO) as well as rutile TaO$_2$ by S-MBE, respectively.

Growing thin films with very high crystalline qualities at growth rates >1 µm h^{-1} by using suboxide molecular beams—with up to 5 µm h^{-1} anticipated growth rates by our model—will make MBE competitive with other established synthesis methods, such as CVD[33] or MOVPE.[34] The T_G that we have demonstrated for high quality Ga$_2$O$_3$ layers grown by S-MBE is significantly lower than what has been demonstrated for the growth of high quality Ga$_2$O$_3$ films by CVD or MOVPE. This makes S-MBE advantageous for BEOL processing. Additionally, Ga$_2$O$_3$ grown with a vast excess of Ga$_2$O (g) and high oxygen activity in Ga$_2$O$_3$-rich mixtures may suppress Ga vacancies in the Ga$_2$O$_3$ layers formed, which are believed to act a compensating acceptors[20,71]—potentially improving the electrical performance of n-type Ga$_2$O$_3$-based devices significantly.

The development of Al + Al$_2$O$_3$ mixtures for the growth of epitaxial Al$_2$O$_3$ and (Al$_x$Ga$_{1-x}$)$_2$O$_3$ at comparably high growth rates by S-MBE is foreseeable. In order to fabricate vertical high-power devices, thin film thicknesses in the micrometer range are desired. S-MBE allows the epitaxy of such devices in relatively short growth times [i.e., within a few hours as demonstrated for Ga$_2$O$_3$(010) in this work] while maintaining nanometer scale smoothness. In addition, the use of an Al$_2$O (g) and Ga$_2$O (g) molecular beams during (Al$_x$Ga$_{1-x}$)$_2$O$_3$ S-MBE may also extend its growth domain toward higher adsorption-controlled regimes—being beneficial for the performance of (Al$_x$Ga$_{1-x}$)$_2$O$_3$-based heterostructure devices.

Our demonstration (not shown in this work) of high quality films of Ga$_2$O$_3$, Ga$_2$O$_3$ doped with SnO, In$_2$O$_3$, ITO, TaO$_2$, LaInO$_3$, and LaAlO$_3$ suggests that this synthesis-science approach—utilizing a combination of thermodynamics to identify which suboxides can be produced in molecular beams in combination with a kinetic model of the growth process—can be applied to a wide-range of oxide compounds.[55] We anticipate S-MBE to be applicable to all materials that form via intermediate reaction products (a *subcompound*). Examples following this reasoning include ZrO$_2$, Pb(Zr,Ti)O$_3$, and (Hf,Zr)O$_2$ all via the supply of a molecular beam of ZrO (predicted by our thermodynamic calculations[55]) Ga$_2$Se$_3$ via Ga$_2$Se,[11,72,73] In$_2$Se$_3$ through In$_2$Se,[11,74,75] In$_2$Te$_3$ by In$_2$Te,[11,76] or Sn$_2$Se via SnSe.[11,77]

DATA AVAILABILITY

The data supporting the findings of this study are available within the paper. Additional data related to the growth and structural characterization are available at https://doi.org/10.34863/a2jw-kh18. Any additional data connected to the study are available from the corresponding author upon reasonable request.

REFERENCES

[1] M. A. Hermann and A. Sitter, *Molecular Beam Epitaxy: Fundamentals and Current Status*, 2nd ed. (Springer, Berlin, 1996), pp. 1–31.

[2] T. Onuma, S. Saito, K. Sasaki, T. Masui, T. Yamaguchi, T. Honda, and M. Higashiwaki, Jpn. J. Appl. Phys., Part 1 **54**, 112601 (2015).

[3] T. Wang, W. Li, C. Ni, and A. Janotti, Phys. Rev. Appl. **10**, 011003 (2018).

[4] M. Higashiwaki, K. Sasaki, A. Kuramata, T. Masui, and S. Yamakoshi, Appl. Phys. Lett. **100**, 013504 (2012).

[5] S. Krishnamoorthy, Z. Xia, C. Joishi, Y. Zhang, J. McGlone, J. Johnson, M. Brenner, A. R. Arehart, J. Hwang, S. Lodha, and S. Rajan, Appl. Phys. Lett. **111**, 023502 (2017).

[6] R. Jinno, C. S. Chang, T. Onuma, Y. Cho, S.-T. Ho, M. C. Cao, K. Lee, V. Protasenko, D. G. Schlom, D. A. Muller, H. G. Xing, and D. Jena, Sci. Adv. **7**, eabd5891 (2021).

[7] M.-Y. Tsai, O. Bierwagen, M. E. White, and J. S. Speck, J. Vac. Sci. Technol., A **28**, 354 (2010).

[8] P. Vogt and O. Bierwagen, Appl. Phys. Lett. **106**, 081910 (2015).

[9] P. Vogt and O. Bierwagen, Appl. Phys. Lett. **108**, 072101 (2016).

[10] P. Vogt, O. Brandt, H. Riechert, J. Lähnemann, and O. Bierwagen, Phys. Rev. Lett. **119**, 196001 (2017).

[11] P. Vogt and O. Bierwagen, Phys. Rev. Mater. **2**, 120401(R) (2018).

[12] P. Vogt, "Growth kinetics, thermodynamics, and phase formation of group-III and IV oxides during molecular beam epitaxy," Ph.D. thesis, Humboldt University of Berlin, 2017.

[13] P. Vogt and O. Bierwagen, Appl. Phys. Lett. **109**, 062103 (2016).

[14] S. Migita, Y. Kasai, H. Ota, and S. Sakai, Appl. Phys. Lett. **71**, 3712 (1997).

[15] R. W. Ulbricht, A. Schmehl, T. Heeg, J. Schubert, and D. G. Schlom, Appl. Phys. Lett. **93**, 102105 (2008).

[16] J. L. MacManus-Driscoll, M. P. Wells, C. Yun, J.-W. Lee, C.-B. Eom, and D. G. Schlom, APL Mater. **8**, 040904 (2020).

[17] O. Bierwagen, M. E. White, M.-Y. Tsai, and J. S. Speck, Appl. Phys. Lett. **95**, 262105 (2009).

[18] H. Paik, Z. Chen, E. Lochocki, A. H. Seidner, A. Verma, N. Tanen, J. Park, M. Uchida, S. Shang, B.-C. Zhou, M. Brützam, R. Uecker, Z.-K. Liu, D. Jena, K. M. Shen, D. A. Muller, and D. G. Schlom, APL Mater. **5**, 116107 (2017).

[19] A. B. Mei, L. Miao, M. J. Wahila, G. Khalsa, Z. Wang, M. Barone, N. J. Schreiber, L. E. Noskin, H. Paik, T. E. Tiwald, Q. Zheng, R. T. Haasch, D. G. Sangiovanni, L. F. Piper, and D. G. Schlom, Phys. Rev. Mater. **3**, 105202 (2019).

[20] E. Korhonen, F. Tuomisto, D. Gogova, G. Wagner, M. Baldini, Z. Galazka, R. Schewski, and M. Albrecht, Appl. Phys. Lett. **106**, 242103 (2015).

[21] H. Peelaers, J. L. Lyons, J. B. Varley, and C. G. Van De Walle, APL Mater. **7**, 022519 (2019).

[22] E. Calleja, M. A. Sánchez-García, F. J. Sánchez, F. Calle, F. B. Naranjo, E. Muñoz, S. I. Molina, A. M. Sánchez, F. J. Pacheco, and R. García, J. Cryst. Growth **201-202**, 296 (1999).

[23] G. Koblmüller, C. S. Gallinat, and J. S. Speck, J. Appl. Phys. **101**, 083516 (2007).

[24] S. Fernández-Garrido, G. Koblmüller, E. Calleja, and J. S. Speck, J. Appl. Phys. **104**, 033541 (2008).

[25] H. Kato, M. Sano, K. Miyamoto, and T. Yao, Jpn. J. Appl. Phys., Part 1 **42**, 2241 (2003).

[26] S. Ghose, M. S. Rahman, J. S. Rojas-Ramirez, M. Caro, R. Droopad, A. Arias, and N. Nedev, J. Vac. Sci. Technol., B **34**, 02L109 (2016).

[27] S. Ghose, S. Rahman, L. Hong, J. S. Rojas-Ramirez, H. Jin, K. Park, R. Klie, and R. Droopad, J. Appl. Phys. **122**, 095302 (2017).

[28] R. Droopad, private communication from Ravi Droopad, the corresponding author of Ref. 27 (2017).

[29] R. H. Lamoreaux, D. L. Hildenbrand, and L. Brewer, J. Phys. Chem. Ref. Data **16**, 419 (1987).

[30] C. J. Frosch and C. D. Thurmond, J. Phys. Chem. **66**, 877 (1962).

[31] G. Hoffmann, M. Budde, P. Mazzolini, and O. Bierwagen, APL Mater. **8**, 031110 (2020).

[32] M. Passlack, Z. Yu, R. Droopad, J. K. Abrokwah, D. Braddock, S.-I. Yi, M. Hale, J. Sexton, and A. C. Kummel, in *III-V Semiconductor Heterostructures: Physics and Devices* (Research Signpost, Kerala, India, 2003), pp. 1–29.

[33] S. Rafique, L. Han, A. T. Neal, S. Mou, J. Boeckl, and H. Zhao, Phys. Status Solidi A **215**, 1700467 (2018).

[34] Y. Zhang, F. Alema, A. Mauze, O. S. Koksaldi, R. Miller, A. Osinsky, and J. S. Speck, APL Mater. **7**, 022506 (2019).

[35] P. Vogt, A. Mauze, F. Wu, B. Bonef, and J. S. Speck, Appl. Phys. Express **11**, 115503 (2018).

[36] B. Heying, R. Averbeck, L. F. Chen, E. Haus, H. Riechert, and J. S. Speck, Appl. Phys. Lett. **88**, 1855 (2000).

[37] N. Gogneau, E. Sarigiannidou, E. Monroy, S. Monnoye, H. Mank, and B. Daudin, Appl. Phys. Lett. **85**, 1421 (2004).

[38] J. Neugebauer, T. K. Zywietz, M. Scheffler, J. E. Northrup, H. Chen, and R. M. Feenstra, Phys. Rev. Lett. **90**, 056101 (2003).

[39] J. Kwo, M. Hong, A. R. Kortan, K. L. Queeney, Y. J. Chabal, R. L. Opila, D. A. Muller, S. N. G. Chu, B. J. Sapjeta, T. S. Lay, J. P. Mannaerts, T. Boone, H. W. Krautter, J. J. Krajewski, A. M. Sergnt, and J. M. Rosamilia, J. Appl. Phys. **89**, 3920 (2001).

[40] O. Bierwagen, A. Proessdorf, M. Niehle, F. Grosse, A. Trampert, and M. Klingsporn, Cryst. Growth Des. **13**, 3645 (2013).

[41] A. Fissel, Z. Elassar, O. Kirfel, E. Bugiel, M. Czernohorsky, and H. J. Osten, J. Appl. Phys. **99**, 074105 (2006).

[42] J. P. Liu, P. Zaumseil, E. Bugiel, and H. J. Osten, Appl. Phys. Lett. **79**, 671 (2001).

[43] T. Watahiki, W. Braun, and H. Riechert, J. Vac. Sci. Technol., B **27**, 262 (2009).

[44] C. P. Chen, M. Hong, J. Kwo, H. M. Cheng, Y. L. Huang, S. Y. Lin, J. Chi, H. Y. Lee, Y. F. Hsieh, and J. P. Mannaerts, J. Cryst. Growth **278**, 638 (2005).

[45] K. Sasaki, A. Kuramata, T. Masui, E. G. Víllora, K. Shimamura, and S. Yamakoshi, Appl. Phys. Express **5**, 035502 (2012).

[46] S. Raghavan, T. Schumann, H. Kim, J. Y. Zhang, T. A. Cain, and S. Stemmer, APL Mater. **4**, 016106 (2016).

[47] G. Hass, J. Am. Ceram. Soc. **33**, 353 (1950).

[48] M. Fernández-Perea, M. Vidal-Dasilva, J. I. Larruquert, J. A. Aznárez, J. A. Méndez, E. Gullikson, A. Aquila, and R. Soufli, J. Appl. Phys. **105**, 353 (2009).

[49] J. Geurts, S. Rau, W. Richter, and F. J. Schmitte, Thin Solid Films **121**, 217 (1984).

[50] V. Kračev, Z. Škraba, M. Hudomalj, and S. Sulčič, Thin Solid Films **129**, L61 (1985).

[51] X. Q. Pan and L. Fu, J. Appl. Phys. **89**, 6048 (2001).

[52] X. Q. Pan and L. Fu, J. Electroceram. **7**, 35 (2001).

[53] W. Guo, L. Fu, Y. Zhang, K. Zhang, L. Y. Liang, Z. M. Liu, H. T. Cao, and X. Q. Pan, Appl. Phys. Lett. **96**, 042113 (2010).

[54] B. Gorbunov, V. Y. Filipchenko, and S. K. Finkel'shtein, Inorg. Mater. **19**, 1239 (1983).

[55] K. M. Adkison, S.-L. Shang, B. J. Bocklund, D. Klimm, D. G. Schlom, and Z.-K. Liu, APL Mater. **8**, 081110 (2020).

[56] M. Passlack, J. K. Abrokwah, and Z. J. Yu, U.S. patent 6,094,295 (2000).

[57] M. Passlack, J. K. Abrokwah, R. Droopad, and C. D. Overgaard, U.S. patent 6,030,453 (2000).

[58] C. B. Alcock, V. P. Itkin, and M. K. Horrigan, Can. Metall. Q. **23**, 309 (1984).

[59] M. Zinkevich and F. Aldinger, J. Am. Ceram. Soc. **87**, 683 (2004).

[60] Scientific Group Thermodata Europe (SGTE), in *Landolt–Börnstein*, New Series, Group IV, edited by Lehrstuhl fuer Theoretische Huettenkunde (Springer-Verlag Berlin Heidelberg, 1999).

[61] J.-O. Andersson, T. Helander, L. Höglund, S. Pingfang, and B. Sundman, Calphad **26**, 273 (2002).

[62] FilMetrics F40, KLA Corporation, San Diego, CA.

[63] C. D. Theis and D. G. Schlom, in *High Temperature Materials Chemistry IX*, edited by K. E. Spear (Electrochemical Society, Pennington, 1997), Vol. 97-39, pp. 610–616.

[64] Y. Oshima, E. Ahmadi, S. Kaun, F. Wu, and J. S. Speck, Semicond. Sci. Technol. **33**, 015013 (2018).

[65] J. Åhman, G. Svensson, and J. Albertsson, Acta Crystallogr., Sect. C **52**, 1336 (1996).

[66] J. Wei, K. Kim, F. Liu, P. Wang, X. Zheng, Z. Chen, D. Wang, A. Imran, X. Rong, X. Yang, F. Xu, J. Yang, B. Shen, and X. Wang, J. Semicond. **40**, 012802 (2019).

[67] C. S. Chang, N. Tanen, V. Protasenko, T. J. Asel, S. Mou, H. G. Xing, D. Jena, and D. A. Muller, arXiv:2012.00263 (2020).

[68] E. Ahmadi, O. S. Koksaldi, X. Zheng, T. Mates, Y. Oshima, U. K. Mishra, and J. S. Speck, Appl. Phys. Express **10**, 071101 (2017).

[69] D. G. Schlom and J. S. Harris, "MBE growth of high Tc superconductors," in *Molecular Beam Epitaxy: Applications to Key Materials*, edited by R. F. C. Farrow (Noyes, Park Ridge, 1995), pp. 541–542.

[70]E. Ahmadi, O. S. Koksaldi, S. W. Kaun, Y. Oshima, D. B. Short, U. K. Mishra, and J. S. Speck, Appl. Phys. Express **10**, 041102 (2017).

[71]T. Zacherle, P. C. Schmidt, and M. Martin, Phys. Rev. B **87**, 023206 (2013).

[72]G. A. Gamal, A. T. Nagat, M. M. Nassary, and A. M. Abou-Alwafa, Cryst. Res. Technol. **31**, 359 (1996).

[73]N. Teraguchi, F. Kato, M. Konagai, K. Takahashi, Y. Nakamura, and N. Otsuka, Appl. Phys. Lett. **59**, 567 (1991).

[74]J. H. Greenberg, V. A. Borjakova, and V. F. Shevelkov, J. Chem. Thermodyn. **5**, 233 (1973).

[75]T. Okamoto, A. Yamada, and M. Konagai, J. Cryst. Growth **175-176**, 1045 (1997).

[76]T. D. Golding, P. R. Boyd, M. Martinka, P. M. Amirtharaj, J. H. Dinan, S. B. Qadri, D. R. T. Zahn, and C. R. Whitehouse, J. Appl. Phys. **65**, 1936 (1989).

[77]V. P. Bhatt, K. Gireesan, and G. R. Pandya, J. Cryst. Growth **96**, 649 (1989).